

# Single-Photon Imaging and Efficient Coupling to Single Plasmons

M. Celebrano, R. Lettow, P. Kukura, M. Agio, A. Renn, S. Götzinger, V. Sandoghdar

*Laboratory of Physical Chemistry and optETH,*

*ETH Zurich, CH-8093 Zurich, Switzerland*

## Abstract

We demonstrate strong coupling of single photons emitted by individual molecules at cryogenic and ambient conditions to individual nanoparticles. We provide images obtained both in transmission and reflection, where an efficiency greater than 55% was achieved in converting incident narrow-band photons to plasmon-polaritons (plasmons) of a silver nanoparticle. Our work paves the way to spectroscopy and microscopy of nano-objects with sub-shot noise beams of light and to triggered generation of single plasmons and electrons in a well-controlled manner.

PACS numbers: 42.50.Ct, 42.50.Ar, 42.30.-d, 78.67.Bf

Coupling of light to dipolar radiators lies at the heart of light-matter interaction. Theoretical studies have predicted more than 80% extinction of a focused classical Gaussian beam by a single dipolar radiator [1, 2], and recent experimental investigations have reported up to 12% extinction of classical light by single quantum emitters [3, 4, 5]. Laboratory realizations of spectroscopy and microscopy on single nano-objects with single-photon illumination, however, have been confronted by obstacles. In particular, excitation of a quantum emitter by individual photons has only been possible in confined geometries [6, 7], and quantum optical imaging [8, 9, 10] of subwavelength structures has not been explored at the single-photon level. One bottle-neck in spectroscopy with single photons is access to bright, tunable, and narrow-band single-photon sources [11]. Another challenge stems from the fundamental wave character of propagating photons which leads to a weak coupling with matter. In this Letter, we demonstrate more than 55% coupling between a diffraction-limited beam of single photons and single silver nanoparticles, which act as classical dipolar antennae. This strong photon-dipole coupling allows efficient excitation of single plasmon-polaritons (plasmons) [12, 13] and imaging of nano-objects with nonclassical light.

The source of single photons in our experiments is a single dye molecule embedded in an organic crystalline matrix. Figure 1a shows the energy level scheme of such a molecule as well as its excitation and fluorescence channels. We begin with experiments performed at  $T \simeq 1.4$  K, where we used a tunable narrow-band dye laser to excite dibenzanthanthrene (DBATT) embedded in n-tetradecane on the  $S_{0,v=0} \rightarrow S_{1,v=1}$  transition at the wavelength of  $\lambda \simeq 581$  nm [14]. This state rapidly decays to the  $S_{1,v=0}$  state that has a lifetime of 9.5 ns determined by fluorescence to the  $S_{0,v}$  states. By filtering the broad Stokes-shifted fluorescence to the  $v \neq 0$  manifold and collecting the emission on the  $S_{1,v=0} \rightarrow S_{0,v=0}$  zero-phonon line (ZPL), we obtained a source of single photons at  $\lambda \simeq 589$  nm with a lifetime-limited linewidth of 17 MHz [14]. Figure 1b displays a recorded second-order autocorrelation function that proves the strongly photon-antibunched nature of this light. More details of the cryogenic setup and characterization of the single-photon source can be found in Ref. [14]. Here, it suffices to point out that this narrow-band single-photon source delivers a high power of up to 500 fW, corresponding to about  $10^6$  detected photons per second.

The collimated beam of single photons was coupled into a single-mode fiber and directed to a home-built microscope at room temperature as shown in Fig. 2a. An oil-immersion objective with a numerical aperture (NA) of 1.4 focused this light onto single silver nanopar-

ticles with nominal diameter of 60 nm (British Biocell), which were spin coated on a glass cover slide and index-matched by immersion in oil (refractive index=1.49). Another microscope objective (NA=1.4) collected the transmitted light and sent it onto an avalanche photodiode (APD). A second APD was used to record the signal in reflection. In addition, we used flip mirrors to couple the light from the dye laser or a white-light source directly to the room-temperature microscope for characterization and diagnostics of the nanoparticles on the sample. By inserting a pinhole in the image plane, we could select each single particle and record its plasmon spectrum using a grating spectrometer.

The red trace in Fig. 2b plots the plasmon spectrum of a nanoparticle that matched our single photon source at  $\lambda = 589$  nm indicated by the black curve. This spectrum corresponds to a prolate silver ellipsoid with a short axis of 46 nm and a long axis of 94 nm that is parallel to the substrate. We find good agreement with the results of calculations that considered a dipolar scatterer [15] and illumination parallel to the long axis of the particle (see blue curve of Fig. 2b). Indeed, electron microscopy revealed that the colloidal particles were mostly elongated (see Fig. 2c) with a notable variation in shape and size. We, thus, selected nanoparticles that matched the wavelength of our single-photon source (see Fig. 2b) and maximized the signal.

Figures 3a and b display images of a nanoparticle recorded simultaneously in transmission and reflection as the sample was scanned by a piezo-electric stage across the focus of the laser beam. The origin of these signals is scattering of the incident light from the nanoparticle [16], and the details of the contrast mechanism and the detection scheme are discussed in the literature [17, 18]. Here, we briefly highlight the interferometric character of the signal  $I_d$

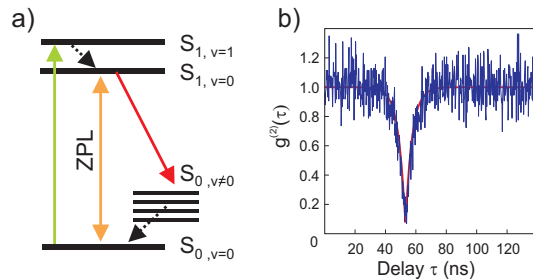


FIG. 1: (a) The energy level scheme of a dye molecule. See text for details. (b) An example of the second-order correlation function of a single DBATT molecule under continuous-wave excitation.

recorded on the detector, which is described as

$$I_d = |E_{\text{ref}} + E_{\text{sca}}|^2 = |E_{\text{ref}}|^2 + |E_{\text{sca}}|^2 - 2|E_{\text{ref}}||E_{\text{sca}}|\sin\varphi. \quad (1)$$

where  $E_{\text{sca}}$  is the electric field of the scattered light at the detector position, and  $E_{\text{ref}}$  denotes the electric field of a “reference” beam. In case of the transmission signal, the reference is the incident light, whereas for the reflection signal, it is produced by a residual reflection of the illumination within the optical setup. Depending on the relation between  $E_{\text{ref}}$  and  $E_{\text{sca}}$ , the second or the third term of Eq. (1) might dominate and determine the signal contrast [18]. Furthermore, this is influenced by the scattering phase angle  $\varphi$ , which depends on the dielectric function of the nanoparticle at the illumination wavelength as well as its size and shape [18].

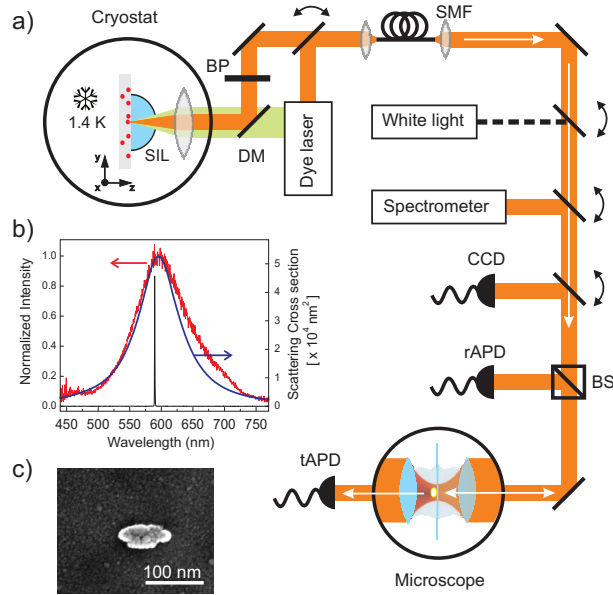


FIG. 2: (a) Single dye molecules embedded in a thin organic matrix at  $T=1.4$  K produce a beam of single photons. This beam is collected and collimated by a solid-immersion lens and an aspherical lens inside the cryostat and then coupled into a single-mode fiber (SMF). The output of this fiber is sent to the sample in a room-temperature microscope. Two avalanche photodiodes rAPD and tAPD register the signal in reflection and transmission, respectively. A spectrometer records the plasmon spectrum of a particle upon illumination by a white-light source. DM: dichroic mirror, BS: beam splitter. (b) The red curve shows the experimentally measured plasmon spectrum of the particle studied in the first experiment. The blue curve displays a theoretical spectrum corresponding to an ellipsoidal silver particle with long and short axes of 94 and 46 nm, respectively. The black curve shows the spectrum of the narrow-band single-photon source. (c) Electron microscope image of a typical silver spheroid.

Next, in Figs. 3d and e we present raster-scan images of the same single nanoparticle recorded under illumination by single photons. As shown by the two cross sections  $\delta$  and  $\epsilon$  in Fig. 3f, we find full width at half-maximum (FWHM) values of 300 nm and 260 nm in transmission and reflection images, respectively. The solid curves display the outcome of rigorous vectorial three-dimensional calculations [15] considering a focused Gaussian beam [2]. Here, the silver nanoparticle was modeled as a dipolar emitter, taking into account radiative and dynamic depolarization corrections [19]. We found a good agreement between the theoretical predictions and the experimental results if we considered the polarizability corresponding to the scattering cross section reported in Fig. 2b [15]. A correction to the observed FWHM,  $\Delta X_{np}$ , for the finite size of the nanoparticle could also be made according to  $\Delta X_{np} \approx \sqrt{(\Delta X_{pd})^2 + D_{np}^2}$  where  $D_{np} = 46$  nm is the particle size along the scan direction, and  $\Delta X_{pd}$  is the FWHM calculated for a point dipole. However, this amounts to an adjustment of only 3 nm, which we have chosen to neglect here. We mention in passing that the appearance of the elliptical images in Figs. 3a,b,d,e is a well-known effect for tightly focused linearly-polarized light [20]. Another noteworthy point is that because of the nearly index-matched sample, the large cross section of the silver particle, and a tight focusing, the reflection signal is dominated by the second term of equation (1) and, therefore, maps the intensity of the incident beam in the focus spot. The transmission signal, on the other hand, has a substantial contribution from the interference term that depends on the electric field of the excitation light, which has a larger spatial extent than the intensity [15]. Indeed a comparison of the data in Figs. 3c and 3f reveals that the FWHMs in transmission are systematically wider than those in reflection images.

Tight focusing is key to achieving a strong coupling between a light field and a dipolar emitter [1, 2, 3]. The cross sections in Fig. 3f reveal large extinction and reflection contrasts of 55% in transmission and 22% in reflection. This is in very good agreement with the rigorous vectorial calculations shown by the solid curves, which take into account the modal character of a Gaussian beam as well as the illumination and collection solid angles [1].

The data presented above clearly show the large effect of a single dipolar oscillator on a propagating light beam. Given that the interaction of the incoming photons with the nanoparticle has been mediated by the excitation of its plasmon-polaritons, these results indicate a high probability that an incident photon excites a single plasmon [13]. To define an efficiency for the conversion of a photon to a plasmon, we add the probabilities that it is

absorbed and scattered by the particle. In general, computation of this quantity from the reflection and transmission measurements requires a careful consideration of the incident focusing angle  $\alpha$  and the collection angle  $\beta$  [1, 2]. However, if  $\alpha = \beta$ , a simple argument based on energy conservation lets us conclude that the sum of the scattered and absorbed powers equals the power removed from the incident beam, which is directly read from the transmission dip. If  $\alpha < \beta$ , some of the light that is scattered at larger angles is also collected, which reduces the transmission dip. In our case, the illumination and collection microscope objectives were identical, but the former was not completely filled in order to minimize the loss of photons. Thus, the data in Fig. 3f yield a lower bound of 55% for the photon-plasmon conversion efficiency.

The two series of images in Fig. 3 acquired with laser light and a single photon source appear nearly identical. However, in the first case the signal can be described by the interference of classical fields, while the contrast mechanism of the images recorded by the latter

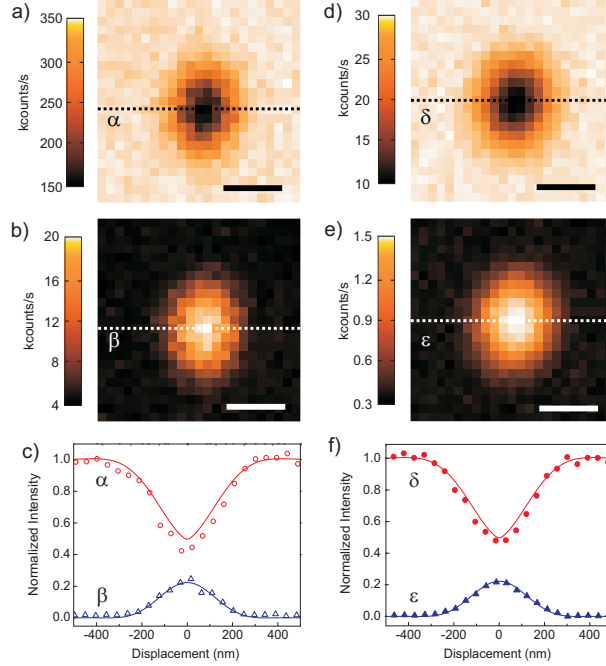


FIG. 3: Transmission (a) and reflection (b) images obtained when the sample was scanned laterally across the focus of a laser beam at a speed of 10 ms per pixel. (c) Cross sections from (a) and (b). Average of 12 transmission (d) and reflection (e) images obtained when the sample was laterally scanned in the focus of the single-photon beam at 40 ms per pixel. (f) Cross sections from (d) and (e). Light beams were polarized along the vertical directions of the images in (a), (b), (d), and (e). Scale bars correspond to 500 nm.

can only be understood as the result of a Young-double-slit type of experiment for single photons [21, 22]. Here, the two interfering paths for each photon correspond to scattering by the nanoparticle and transmission without any interaction. After averaging the signal accumulated from a large number of single photons at each pixel, one retrieves the results familiar from classical optics.

We have demonstrated that a focused beam of single photons can be used to detect and image nanoparticles. This beam can also be produced in a triggered fashion by using a pulsed excitation of the molecule on the  $S_{0,v=0} \rightarrow S_{1,v=1}$  transition [23]. If the excitation beam is strong enough, one can ensure the production of a photon after each pulse, yielding an intensity-squeezed light source with a well-defined number of photons per unit time. Such a light source would allow the detection of objects with arbitrarily small optical contrast because it eliminates noise on the first term  $|E_{\text{ref}}|^2$  of Eq. (1) so that the second and third terms can be deciphered regardless of their magnitudes [11, 18, 24]. One should bear in mind, however, that any loss in the optical system reduces the degree of squeezing [8]. In our experiment, the central source of loss has been the limited collection angle of the lens used behind the solid-immersion lens in the cryostat (see Fig. 2a). This can be substantially improved by employing different choices of lenses [25].

A second major cause for losses in the setup of Fig. 2a is the coupling into an optical fiber. To verify that use of a single mode and spatial mode filtering is not a strict requirement for the ability to focus single photons to the diffraction limit, we also performed free-beam measurements. Here, we collimated the single photon emission of a room-temperature terrylene molecule embedded in a thin para-terphenyl film [26, 27], and sent it directly to the second microscope as described earlier in Fig. 2a. Figure 4a displays an example of an image of a silver nanoparticle recorded in this fashion, while Fig. 4b shows a cross section from it. We find that the full width at half-maximum is as small as 370 nm [28], demonstrating that freely propagating single photons can be indeed focused tightly. Here, the transmission dip amounts to only 15% because in this experiment we did not search for a nanoparticle with a plasmon resonance that matched the emission spectrum of terrylene. Moreover, the photon-plasmon coupling efficiency in this arrangement is less efficient than the narrow-band single photon source discussed earlier because the broad room-temperature emission of terrylene (see inset in Fig. 4b) does not fully overlap with the particle plasmon resonance.

Strong focusing of single photons demonstrated in this work opens doors to many inter-

esting experiments where photons are to be managed with high efficiency and funneled to other quantum systems in the condensed phase. For example, one can use a silver nanoparticle as a nanoantenna [29] to convert single propagating photons to single plasmons in nano-circuits. As opposed to the near-field coupling of photons from pre-positioned emitters to nanowires [12], coupling via propagating beams has the great advantage of being versatile with potential for broad-band communication because a large number of narrow-band single photon beams can be coupled simultaneously or sequentially via the same nano-antenna port. Plasmons can in turn generate electrons in a photovoltaic process where a quantum of excitation at optical frequencies gives birth to an electron [30]. These processes would offer interesting possibilities for quantum state engineering of hybrid systems. Another important promise of our work is in the detection and imaging of very small nanoparticles and single molecules [11, 18, 31]. To achieve this, we plan to optimize the use of solid-immersion lenses to reach collection efficiencies in excess of 90% [25], and thus produce an intensity-squeezed train of single photons from a single molecule.

We thank J. Hwang; N. Mojarad, and G. Zumofen for fruitful discussions. This work was

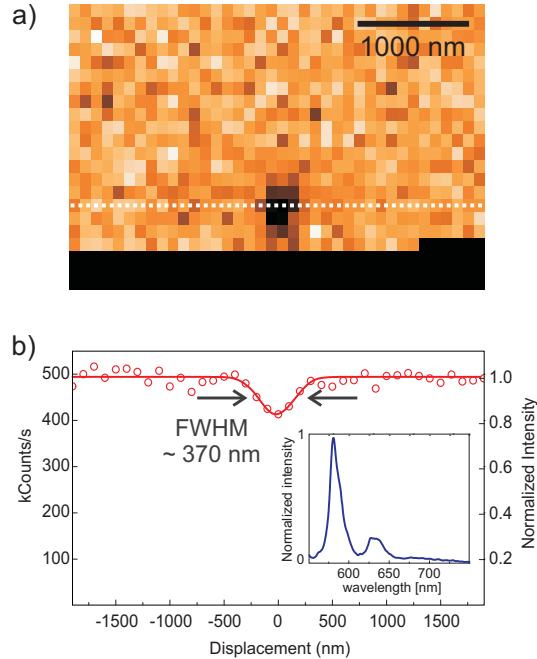


FIG. 4: a) A raster-scan image of a silver nanoparticle illuminated by single photons from a terrylene molecule at room temperature. The black region at the bottom indicates loss of signal caused by the photobleaching of the molecule. b) A cross section from part (a). The inset displays the emission spectrum of a single terrylene molecule.



funded by the Swiss National Science Foundation (SNF).

---

- [1] G. Zumofen, N. M. Mojarad, V. Sandoghdar, and M. Agio, Phys. Rev. Lett. **101**, 180404 (2008).
- [2] N. Mojarad, G. Zumofen, V. Sandoghdar, and M. Agio, J. Euro. Opt. Soc. **4**, 09014 (2009).
- [3] G. Wrigge, I. Gerhardt, J. Hwang, G. Zumofen, and V. Sandoghdar, Nature Phys. **4**, 60 (2008).
- [4] A. N. Vamivakas, *et al.*, Nano Letters **7**, 2892 (2007).
- [5] M. K. Tey, *et al.*, Nature Phys. p. doi:10.1038/nphys1096 (2008).
- [6] J. Eschner, C. Raab, F. Schmidt-Kaler, and R. Blatt, Nature **413**, 495 (2001).
- [7] G. Rempe, *et al.*, in *Coherence and Quantum Optics VIII*, edited by N. P. Bigelow, J. H. Eberly, C. R. Stroud, and I. A. Walmsley (Kluwer Academic / Plenum Publishers, New York (2003), 2007), pp. 241–248.
- [8] M. I. Kolobov, Rev. Mod. Phys. **71**, 1539 (1999).
- [9] N. Treps, *et al.*, Phys. Rev. Lett. **88**, 203601 (2002).
- [10] L. Lugiato, A. Gatti, and E. Brambilla, J. Opt. B **4**, S176 (2002).
- [11] B. Lounis and M. Orrit, Rep. Prog. Phys. **68**, 1129 (2005).
- [12] A. V. Akimov, *et al.*, Nature **450**, 402 (2007).
- [13] M. S. Tame, *et al.*, Phys. Rev. Lett. **101**, 190504 (2008).
- [14] R. Lettow, *et al.*, Opt. Express **15**, 15842 (2007).
- [15] Supplementary materials
- [16] C. F. Bohren and D. R. Huffman, *Absorption and Scattering of Light by Small Particles* (John Wiley and Sons, 1983).
- [17] A. A. Mikhailovsky, M. A. Petruska, M. I. Stockman, and V. I. Klimov, Opt. Lett. **28**, 1686 (2003).
- [18] K. Lindfors, T. Kalkbrenner, P. Stoller, and V. Sandoghdar, Phys. Rev. Lett. **93**, 037401 (2004).
- [19] M. Meier and A. Wokaun, Opt. Lett. **8**, 581 (1983).
- [20] B. Richards and E. Wolf, Proc. Roy. Soc. London Ser A **235**, 358 (1959).
- [21] G. I. Taylor, Proc. Cambridge Philos. Soc. **15**, 114 (1909).

- [22] L. M. Davis, Phys. Rev. Lett. **60**, 1258 (1988).
- [23] V. Ahtee, *et al.* , J. Mod. Opt. **56**, 161 (2009).
- [24] G. Wrigge, J. Hwang, I. Gerhardt, G. Zumofen, and V. Sandoghdar, Opt. Express **16**, 17358 (2008).
- [25] K. Koyama, M. Yoshita, M. Baba, T. Suemoto, and H. Akiyama, Appl. Phys. Lett. **75**, 1667 (1999).
- [26] R. J. Pfab, J. Zimmermann, C. Hettich, I. Gerhardt, A. Renn, and V. Sandoghdar, Chem. Phys. Lett. **387**, 490 (2004).
- [27] B. Lounis and W. E. Moerner, Nature **407**, 491 (2000).
- [28] This value is larger than that expected from a simple estimate of the diffraction limit because of 1) the inherently larger FWHM that is obtained in transmission measurements and 2) the lower effective numerical aperture due a smaller beam diameter in this experiment.
- [29] M. W. Knight, N. K. Grady, R. Bardhan, F. Hao, P. Nordlander, and N. J. Halas, Nano Lett. **8**, 2346 (2007).
- [30] A. L. Falk, *et al.* , Nature Phys. **5**, 475 (2009).
- [31] P. Kukura, M. Celebrano, A. Renn, and V. Sandoghdar, Nano Lett. **9**, 926 (2009).